Nonlinear mass and heat transfer across liquid-vapor interfaces

Pouria Feyzi Oskouei and Henning Struchtrup

2025

Nonlinear mass and heat transfer across liquid-vapor interfaces

Pouria Feyzi Oskouei and Henning Struchtrup*

Department of Mechanical Engineering, University of Victoria, PO Box 1700 STN CSC, Victoria, British Columbia, Canada V8W 2Y2

(Received 1 May 2025; accepted 24 July 2025; published 12 August 2025)

Nonlinearities in mass and heat transfer across liquid-vapor interfaces are studied based on models from irreversible thermodynamics and the kinetic theory of gases. Specifically, we present the nonlinear extension of the well-known Hertz-Knudsen-Schrage (HKS) model of kinetic theory for mass flux and a corresponding relation for heat transfer. It is shown that this extended model stands in good agreement with established kinetic theory models for zero heat flux. The extended HKS model is linked to the force-flux relations of nonequilibrium thermodynamics by determining their nonlinear interface resistivities, which depend not only on the interface temperature, but also on mass and heat flux. Nondimensionalization based on temperature and saturation pressure yields resistivities independent of the local temperature. Reevaluation of recent Molecular Dynamics data for resistivities [Homes and Vrabec, Phys. Fluids **36**, 022122 (2024)] reveals distinct nonlinearities.

DOI: 10.1103/wzz4-d6sg

I. INTRODUCTION

Evaporation and condensation processes are common both in everyday experience and in many technological systems, such as vapor power plants and refrigeration systems [1]. Despite their prevalence, the microscopic mechanisms and thermodynamic principles governing the processes at liquid-vapor interfaces, particularly under nonequilibrium conditions, remain an area of ongoing investigation and limited understanding.

Experimental observations have revealed notable temperature discontinuities and pressure deviations at the liquid-vapor interface during evaporation and condensation processes. Although these deviations are mostly visible in microscopic systems, remarkable temperature jumps were observed in macroscopic experiments [2–7], challenging traditional hydrodynamic theories and earlier kinetic theory–based models that predicted smaller variations [8–12]. More recent high-precision evaporation experiments yield results that stand in good agreement with classical kinetic theory models [13].

However, the assessment of physical experiments frequently struggles with substantial measurement inaccuracies. Specifically, errors in measuring pressure can equal or surpass the expected deviations from the saturation pressures observed in experimental results [5,14].

Molecular dynamics (MD) simulations study heat and mass transfer at the liquid-vapor interface with molecular-level resolution. These simulations mimic the experimental settings with a stationary interface, where vapor particles are pumped out and returned into the liquid. Unlike physical experiments, which are limited in capturing microscopic details, MD simulations provide direct access to resolved thermodynamic properties, such as density, temperature, pressure, etc. Similar to physical experiments, these simulations have shown a large temperature difference between the bulk regions of liquid and vapor [15,16].

The desire to understand the observations in experiments and MD simulations has sparked interest in refining thermodynamic models, particularly those focusing on interfacial resistivities and phase conversion coefficients [17].

The thermodynamic description of nonequilibrium interfaces is based on the principles of linear irreversible thermodynamics (LIT) [17]. This approach posits linear relationships between thermodynamic fluxes (of mass and energy) and their corresponding forces, i.e., the differences in chemical potentials and temperatures between the adjacent liquid and vapor bulk phases. Within the framework of LIT, interface resistivities, which typically are assumed to only depend on interface temperature, are used to linearly connect forces and fluxes. Recently it was proposed that nonlinear force-flux relations might be required for processes in strong nonequilibrium [18]. The evaluation of this claim is one topic of this contribution.

Although LIT assumes small deviations from equilibrium to maintain linearity between forces and fluxes, MD simulations often exhibit significantly large evaporation and heat fluxes [15]. This raises the possibility that such high fluxes influence resistivities under conditions of intense nonequilibrium, contrasting with the linear regime where resistivities are solely functions of the local state [18].

Within the kinetic theory of gases, the expressions for interface mass and energy fluxes are derived through approximate solutions of the Boltzmann equation and suitable models for the liquid-vapor interface, e.g., via the Chapman-Enskog expansion or moment methods [19,20]. These require an understanding of microscopic condensation probabilities, which are classically assumed to be constant [8,9,11,21–23]. However, some MD simulations suggest that these probabilities vary with vapor particle impact energy and liquid surface temperature [24–28].

*Contact author: struchtr@uvic.ca

In the following, the behavior of liquid-vapor interfaces is studied under the assumption that the vapor is an ideal gas. We present the nonlinear extension of the well-known Hertz-Knudsen-Schrage (HKS) model [8–10], which includes an expression for interfacial heat transfer [23]. Based on this, macroscopic interface relations are derived and studied within the framework of LIT. It is shown that under weak nonequilibrium conditions, resistivities are constant. However, for stronger nonequilibrium with higher fluxes, resistivities must also depend on the fluxes themselves, as proposed in Ref. [18]. We show that nonlinear resistivities are unique in single-flux settings where either mass or heat flux vanishes, but for general cases with both fluxes present their determination is ambiguous. An optimization algorithm is used to determine a solution with continuous resistivities for a large parameter range that agrees with the single-flux and equilibrium cases, but is not unique.

Finally, detailed evaluation of recent MD simulations [15] of single-flux cases gives evidence of nonlinearities in the force-flux relations.

The remainder of this paper is structured as follows: Section II discusses the setup and the bulk equations, followed by a discussion of macroscopic and microscopic sharp interface models. Linear Irreversible Thermodynamics provides the general framework [17], introducing interface resistivities as parameters that in principle can be determined from experimental data. We detail the dimensionless formulation [23,29], which by reducing the influence of interface temperature and saturation pressure provides a clearer view on the behavior of measured properties and the resistivities.

Turning to kinetic theory models, the nonlinear extension of the HKS model (eHKS model) is presented [8–10,12,23], including the heat-transfer expression, in dimensional and dimensionless forms. Due to simplifying assumptions, the eHKS model does not account for Knudsen layer effects [23], but nevertheless includes all relevant physics in good approximation. For comparison, we also present the Ytrehus-Cercignani (Y-C) model for pure evaporation [30,31], which does account for Knudsen layers. While in the eHKS model condensation and accommodation coefficients can be chosen freely, the Y-C model is restricted to a condensation coefficient of unity.

Section III discusses the determination of dimensionless resistivities from the eHKS model for a wide range of process parameters. First, close-to-equilibrium processes are considered to validate the method against established literature [8–10,12,23,32]. Nonlinear resistivities for evaporation are shown to be in good agreement to the Y-C model. Subsequently, the general case is explored, with both fluxes induced simultaneously, to demonstrate the nonlinear interplay and influence of both fluxes on resistivities. Implications of ambiguity and nonuniqueness are discussed.

Section IV evaluates nonlinearities in recent MD simulations for single-flux cases [15], which become particularly apparent when considering the results in dimensionless form. The results highlight that under the strong nonequilibrium conditions of the simulations, resistivities not only vary with the local state but are also influenced by the fluxes in the process. While due to noise and uncertainty in the MD results a full fit to the eHKS model is not possible, we give evidence of principal agreement of behavior.

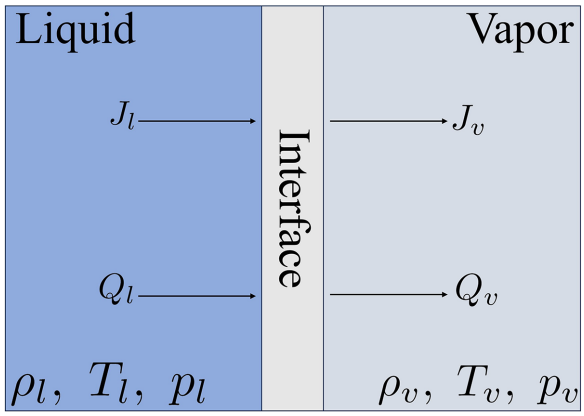

FIG. 1. Schematic of liquid-vapor bulk regions with the interface in nonequilibrium with mass flux J and total energy flux Q passing the interface. In steady state the fluxes in both phases agree, $J = J_l = J_v$, $Q = Q_l = Q_v$.

Finally, Sec. V presents our conclusion and recommendations for future research.

This paper summarizes the M.Sc. thesis of the first author [33].

II. MACROSCOPIC AND MICROSCOPIC INTERFACE MODELS

A. Linear irreversible thermodynamics

We focus on one-dimensional, steady-state processes with a planar interface separating the liquid and vapor bulk regions. Mass and heat transfer occur perpendicular to the interface, with the system considered in a reference frame where the interface remains stationary as sketched in Fig. 1. To differentiate between the two phases, subscripts l for liquid and v for vapor are used, respectively, so that for the liquid region ρ_l is mass density, T_l is temperature, and p_l is pressure; correspondingly for the vapor regions, ρ_v, T_v, and p_v.

Microscopically the interface layer has a diffusive structure with a width of a few molecular diameters, in nonequilibrium followed by a Knudsen layer with width of the order of the mean free path of the vapor. Both in thermodynamics and kinetic theory modeling the structure is not resolved, i.e., the interface is considered as a sharp transition from liquid to vapor. It is assumed that liquid and vapor in the bulk phases are in local thermodynamic equilibrium as described by the Navier-Stokes-Fourier equations [19,29]; that is, the width of the interfacial region (including the Knudsen layer) is effectively ignored.

In one-dimensional steady-state processes the overall mass flux $J = \rho v$, where v denotes flow velocity, momentum flux, P, and energy flux, Q, are constant. All flows are in the direction normal to the liquid-vapor interface. For most evaporation or condensation processes, velocities are relatively small, hence, higher orders of velocity in the balance of momentum and energy are typically ignored, as are viscous stresses. Then, the conservation laws for mass, momentum, and energy

read [17,29,32]

$$J = J_l = J_v, \tag{1}$$

$$P = p_l = p_v, \tag{2}$$

$$Q = Jh_l + q_l = Jh_v + q_v. \tag{3}$$

Here, h and q denote specific enthalpy and nonconvective energy flux, i.e., heat flux, respectively.

Evaporation and condensation processes are generally irreversible. Application of the second law of thermodynamics across the interface gives the interfacial entropy generation rate as

$$\sigma = J(s_v - s_l) + \frac{q_v}{T_v} - \frac{q_l}{T_l} \geqslant 0, \tag{4}$$

where s denotes entropy and $\frac{q}{T}$ is the bulk conductive entropy flux [17,29]. The entropy generation rate vanishes in liquid-vapor equilibrium states and assumes positive values in nonequilibrium.

By eliminating the conductive heat flux in the liquid, q_l, between (3) and (4) the entropy generation rate becomes

$$\sigma = J\left[\frac{g_l}{T_l} - \frac{g_v}{T_v} + h_v\left(\frac{1}{T_v} - \frac{1}{T_l}\right)\right] + q_v\left[\frac{1}{T_v} - \frac{1}{T_l}\right] \geqslant 0, \tag{5}$$

where $g = h - Ts$ denotes Gibbs free energy.

To proceed, we follow the principles of LIT [17,29] where the entropy generation rate is interpreted as a sum of products of thermodynamic fluxes and forces,

$$\sigma = \sum_\alpha \mathcal{J}_\alpha \mathcal{F}_\alpha \geqslant 0, \tag{6}$$

where we identify the fluxes as

$$\mathcal{J}_\alpha = \{J,\ q_v\}, \tag{7}$$

and the forces as

$$\mathcal{F}_\alpha = \{\mathcal{F}_J, \mathcal{F}_q\} = \left\{\frac{g_l}{T_l} - \frac{g_v}{T_v} + h_v\left(\frac{1}{T_v} - \frac{1}{T_l}\right), \frac{1}{T_v} - \frac{1}{T_l}\right\}. \tag{8}$$

Thermodynamic forces describe the deviation from thermodynamic equilibrium, and thermodynamic fluxes are driving the system towards equilibrium. In thermodynamic equilibrium fluxes and forces vanish.

The entropy generation rate must be non-negative for all processes, and vanish in equilibrium. In LIT this is guaranteed by a linear phenomenological ansatz,

$$\mathcal{F}_\alpha = \sum_\beta r_{\alpha\beta}\mathcal{J}_\beta, \tag{9}$$

with the positive semidefinite matrix of resistivities $r_{\alpha\beta}$, which is expected to be symmetric due to Onsager's principle [17,23,34–37].

Typically, in LIT it is assumed that the resistivity matrix depends on the local temperature only, for which one either chooses the temperature of the liquid at the interface (T_l), or a separate interface temperature (T_s). The detailed discussion in Ref. [18] showed that both temperatures are expected to be rather close, and in the following we consider the liquid temperature T_l as the relevant temperature for the description of the interface.

Moreover, in Ref. [18] it was shown that for cases of strong equilibrium, that is, for relatively large fluxes or forces, the resistivities will depend not only on the local equilibrium state through the chosen temperature, but also on the local nonequilibrium state through the fluxes passing the interface. This resulted from describing the interface as an autonomous thermodynamic system with internal variables, that account for changes within the interface induced by processes. LIT modeling of the interaction of the interface with liquid and vapor yielded interface relations similar to Eq. (9) with a symmetric 4×4 matrix of resistivities. The evaluation showed that the internal variables are triggered by heat and mass fluxes through the interface. Due to its small thickness the interface will quickly assume steady states, for which the effect of the internal variables is tantamount to describing the exchange between liquid and vapor via the interface through the LIT relation (9) with a symmetric matrix of flux-dependent resistivities. In what follows it will be seen that the notion of flux-dependent resistivities stands in agreement with nonlinear interface models from kinetic theory.

To proceed, we use the liquid temperature to rewrite the force-flux relation (9) with a dimensionless matrix of resistivities $\hat{r}_{\alpha\beta}$, defined as [23,38]

$$\hat{r}_{11} = \frac{p_{\mathrm{sat}}(T_l)}{R\sqrt{2\pi RT_l}} r_{11}, \quad \hat{r}_{12} = \frac{p_{\mathrm{sat}}(T_l)T_l}{\sqrt{2\pi RT_l}} r_{12},$$

$$\hat{r}_{21} = \frac{p_{\mathrm{sat}}(T_l)T_l}{\sqrt{2\pi RT_l}} r_{21}, \quad \hat{r}_{22} = \frac{p_{\mathrm{sat}}(T_l)RT_l^2}{\sqrt{2\pi RT_l}} r_{22}, \tag{10}$$

where $p_{\mathrm{sat}}(T_l)$ denotes the equilibrium saturation pressure of the evaporating fluid and R is its gas constant. The factor $\sqrt{2\pi}$ is inspired by the typical expressions of kinetic theory, which are shown later in this section.

Correspondingly, the dimensionless mass and heat fluxes are introduced as

$$\hat{J} = \frac{\sqrt{2\pi RT_l}}{p_{\mathrm{sat}}(T_l)} J, \quad \hat{q}_v = \frac{\sqrt{2\pi RT_l}}{p_{\mathrm{sat}}(T_l)} \frac{q_v}{RT_l}. \tag{11}$$

With the dimensionless resistivities and fluxes, the force-flux relations assume the form

$$\begin{bmatrix}\hat{\mathcal{F}}_J \\ \hat{\mathcal{F}}_q\end{bmatrix} = \begin{bmatrix}\frac{g_l}{RT_l} - \frac{g_v}{RT_v} + h_v\left(\frac{1}{RT_v} - \frac{1}{RT_l}\right) \\ \frac{T_l}{T_v} - 1\end{bmatrix} = \begin{bmatrix}\hat{r}_{11} & \hat{r}_{12} \\ \hat{r}_{21} & \hat{r}_{22}\end{bmatrix}\begin{bmatrix}\hat{J} \\ \hat{q}_v\end{bmatrix}, \tag{12}$$

where also the revised forces $\hat{\mathcal{F}}_\alpha$ are dimensionless.

Under the assumptions of a monatomic ideal gas for the vapor, an incompressible liquid, and negligible specific volume of the liquid, v_l, compared to that of the vapor, v_v, the force-flux relations reduce to (see Appendix A)

$$\begin{bmatrix}\hat{\mathcal{F}}_J \\ \hat{\mathcal{F}}_q\end{bmatrix} = \begin{bmatrix}\frac{5}{2}(1 - \Theta + \ln\Theta) - \ln\Pi \\ \frac{1}{\Theta} - 1\end{bmatrix} = \begin{bmatrix}\hat{r}_{11} & \hat{r}_{12} \\ \hat{r}_{21} & \hat{r}_{22}\end{bmatrix}\begin{bmatrix}\hat{J} \\ \hat{q}_v\end{bmatrix}, \tag{13}$$

where temperature and pressure ratios were introduced as

$$\Theta = \frac{T_v}{T_l} = 1 + \Delta\hat{T}, \quad \Pi = \frac{p}{p_{\rm sat}(T_l)} = 1 + \Delta\hat{p}, \tag{14}$$

and the dimensionless temperature jump and pressure deviations are defined as

$$\Delta\hat{T} = \frac{T_v - T_l}{T_l}, \quad \Delta\hat{p} = \frac{p - p_{\rm sat}(T_l)}{p_{\rm sat}(T_l)}. \tag{15}$$

The above relations (12) and (13) reduce significantly for the case of small deviations from equilibrium, for which Taylor expansion and use of thermodynamic property relations lead to [29]

$$\begin{bmatrix} -\Delta\hat{p} \\ -\Delta\hat{T} \end{bmatrix} = \begin{bmatrix} \hat{r}_{11} & \hat{r}_{12} \\ \hat{r}_{21} & \hat{r}_{22} \end{bmatrix} \begin{bmatrix} \hat{J} \\ \hat{q}_v \end{bmatrix}. \tag{16}$$

LIT does not provide further insight into the resistivities $\hat{r}_{\alpha\beta}$, which must be determined either from experimental measurements or refined, i.e., microscopic, models.

With four resistivities (or three, assuming Onsager symmetry [17,35]) in the two governing equations (13), it is not possible to determine all resistivities from a single experiment or simulation. To address this, often simplified process settings are used where either $\hat{J} = 0$ or $\hat{q}_v = 0$, allowing for the determination of two resistivities in a single experiment. These configurations are commonly applied in MD simulations; e.g., see [15,39]. However, it is important to note that such settings do not allow for a complete investigation of the nonlinearity of the force-flux relations.

B. Interface models in kinetic theory

The evaluation of physical experiments often encounters significant measurement errors. Notably, the error associated with pressure measurement can be as large, if not larger, than the anticipated experimental deviation from saturation pressures [5,14]. Moreover, these experiments are generally limited to relatively low fluxes. Consequently, theoretical approaches serve as alternatives for determining resistivities.

In the intuitive Maxwell interface model, one considers simplified processes for vapor particles as follows [23,32]: The condensation coefficient ψ is defined as the probability that a vapor particle will condense upon reaching the interface; this process is depicted in Fig. 2 by the vertical arrow pointing towards the interface. Conversely, the probability that a particle is reflected rather than condensing is $1 - \psi$, accounting for the reflected molecules shown in Fig. 2. In the Maxwell model, rebounding molecules are either specularly or diffusively reflected. In a specular reflection, the normal momentum is inverted while tangential momentum and energy are conserved, whereas in a diffusive reflection, the particle engages in thermal exchange with the particles in the interface before returning into the vapor. The accommodation coefficient γ is defined as the relative amount of diffuse reflections, i.e., $\gamma = 0$ and $\gamma = 1$ indicate pure specular and pure diffuse reflection, respectively. Finally, particles evaporate spontaneously, with the microscopic evaporation coefficient equal to the condensation coefficient [23].

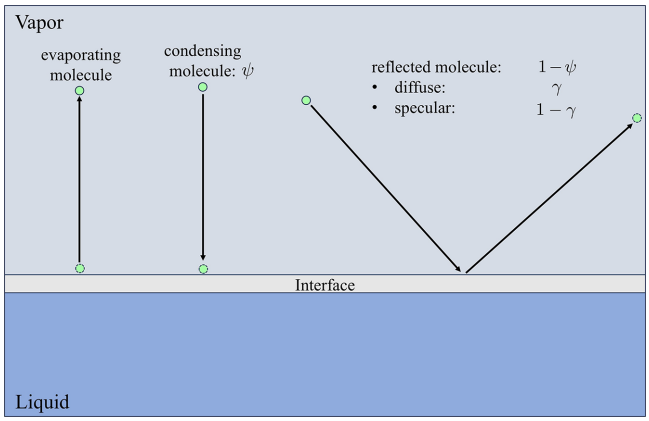

FIG. 2. Vapor particle interactions at the liquid-vapor interface.

One of the most celebrated interface models is the classical HKS model [8–10], which relies on constant condensation and accommodation coefficients. For the classical HKS model, the mass flux is obtained as

$$J = \frac{2\psi}{2-\psi}\left[\frac{p_{\rm sat}(T_l)}{\sqrt{2\pi R T_l}} - \frac{p}{\sqrt{2\pi R T_v}}\right]. \tag{17}$$

Typically, the HKS model considers only mass flux. However, for the full evaluation of evaporation and condensation processes, interface conditions are required for the fluxes of mass *and* energy [32]. Thus, the classical HKS model must be completed with an expression for the heat flux, which for the Maxwell model is obtained as [23,32]

$$\begin{aligned}\frac{q_v}{RT_l} = {} & \frac{2\psi}{2-\psi}\left(2 - \frac{5}{2}\frac{T_v}{T_l}\right)\left[\frac{p_{\rm sat}(T_l)}{\sqrt{2\pi R T_l}} - \frac{p}{\sqrt{2\pi R T_v}}\right] \\ & + 4\frac{\gamma + \psi(1-\gamma)}{2-\gamma-\psi(1-\gamma)}\frac{p}{\sqrt{2\pi R T_v}}\left[1 - \frac{T_v}{T_l}\right].\end{aligned} \tag{18}$$

We emphasize that omission of the relation for heat flux gives an incomplete model. In case that heat flux is small and can be ignored, the heat-flux equation (18) yields a relation between temperatures and pressures that is required for the full analysis of evaporation processes. The criticism of Hertz-Knudsen models in Ref. [40, p. 66] results from this omission.

The HKS equations (17) and (18) are valid only for sufficiently small mass fluxes. To extend their validity, we reconsidered their derivation in Ref. [23] to account for nonlinear terms in flow velocity (see Appendix B for some detail). The resulting eHKS equations include explicit nonlinear terms in the mass flux J.

The eHKS equation for mass flux includes an additional quadratic term,

$$J = \frac{2\psi}{2-\psi}\left[\frac{p_{\rm sat}(T_l)}{\sqrt{2\pi R T_l}} - \frac{p}{\sqrt{2\pi R T_v}} - \frac{1}{2\sqrt{2\pi}}\frac{\sqrt{RT_v}}{p_v}J^2\right], \tag{19}$$

and the eHKS heat flux includes quadratic and quartic terms,

$$\begin{aligned}\frac{q_v}{RT_l} &= \frac{2\psi}{2-\psi}\left(2-\frac{5}{2}\frac{T_v}{T_l}\right)\left[\frac{p_{\rm sat}(T_l)}{\sqrt{2\pi RT_l}}-\frac{p}{\sqrt{2\pi RT_v}}\right]\\ &+4\frac{\gamma+\psi(1-\gamma)}{2-\gamma-\psi(1-\gamma)}\frac{p}{\sqrt{2\pi RT_v}}\left[1-\frac{T_v}{T_l}\right]\\ &+\frac{1}{2}\frac{\gamma+\psi(1-\gamma)}{2-\gamma-\psi(1-\gamma)}\left[\frac{1-\psi}{2-\psi}\frac{8\gamma}{\gamma+\psi(1-\gamma)}\right.\\ &\times\left(\frac{p}{\sqrt{2\pi RT_v}}\left(1-\frac{7T_v}{4T_l}\right)\right.\\ &\left.\left.+\frac{1}{2}\frac{p_{\rm sat}(T_l)}{\sqrt{2\pi RT_l}}\frac{T_v}{T_l}\right)-\frac{T_v}{T_l}\left(\frac{p}{\sqrt{2\pi RT_v}}+2\frac{p_{\rm sat}(T_l)}{\sqrt{2\pi RT_l}}\right)\right]\\ &\times\frac{RT_v}{p^2}J^2+\frac{1}{\sqrt{8\pi}}\frac{\psi}{2-\psi}\frac{(RT_v)^{5/2}}{p^3}\frac{J^4}{RT_l}. \end{aligned}\tag{20}$$

Specifically, in the derivation of this model Knudsen layers were ignored, which introduces some deviation in comparison to more detailed kinetic theory computations [31,41]. Nevertheless, the model is useful for our purpose, since it provides explicit nonlinear force-flux relations for further evaluation. In this context we point out that there is a distinct lack of accurate data from experiments or simulations to verify relations such as the above, or determine meaningful values of the underlying microscopic coefficients (ψ,γ). As will be seen, the model stands in good agreement with more refined models, but is more complete. As such, it provides a first step for the deeper examination of general nonlinearities at phase interfaces.

While evaporation and accommodation coefficients are intuitive in principle, they describe individual microscopic interactions of particles and thus cannot be directly measured in experiments. Instead, macroscopic experiments as well as MD simulations determine collective macroscopic properties such as temperatures, densities, pressures, and heat and mass fluxes, which can only be linked to the microscopic interface coefficients through models such as the above.

Often kinetic theory models rely on condensation and accommodation coefficients as constants [22]. For example, in the original Hertz-Knudsen theory, the condensation coefficient is assumed to be unity [8,9], as well more recent studies conclude that an evaporation coefficient of unity suffices [39]. Other authors argue that the coefficients should not only be dependent on temperature but also that the condensation coefficient should depend as well on the impact velocity of vapor particles [24,25,27,28]. While the above model can be extended to these cases [23,32], we refer further discussion of this to the future.

The eHKS flux relations (19) and (20) are inherently nonlinear functions of the bulk liquid and vapor properties adjacent to the interface, resulting in nonlinearity between forces and fluxes. The next step is to determine resistivities from these relations, for the linear and nonlinear cases.

C. Dimensionless eHKS expressions

For the further evaluation of resistivities based on the eHKS model it is convenient to consider these relations in dimensionless formulation, where—naturally—we use the same expressions as for LIT; that is, the dimensionless temperature and pressure ratios (14) and the dimensionless fluxes (11).

The dimensionless eHKS mass flux expression reads at first

$$\hat{J}=\frac{2\psi}{2-\psi}\left[1-\frac{\Pi}{\sqrt{\Theta}}-\frac{1}{4\pi}\frac{\sqrt{\Theta}}{\Pi}\hat{J}^2\right].\tag{21}$$

To proceed, we solve the quadratic equation (21) for $\hat{J}$. Only one of the two solutions is physically meaningful, since the equilibrium condition $(\Delta\hat{T}=0,\ \Delta\hat{p}=0\rightarrow\hat{J}=0)$ must be satisfied, hence we have

$$\hat{J}=\pi\frac{2-\psi}{\psi}\frac{\Pi}{\sqrt{\Theta}}\left[\sqrt{1-\frac{1}{\pi}\left(\frac{2\psi}{2-\psi}\right)^2\left(1-\frac{\sqrt{\Theta}}{\Pi}\right)}-1\right].\tag{22}$$

Again utilizing (11), (14), and (20), the dimensionless heat flux reduces to

$$\begin{aligned}\hat{q}_v &= \frac{2\psi}{2-\psi}\left(2-\frac{5}{2}\Theta\right)\left[1-\frac{\Pi}{\sqrt{\Theta}}\right]+4\frac{\gamma+\psi(1-\gamma)}{2-\gamma-\psi(1-\gamma)}\frac{\Pi}{\sqrt{\Theta}}(1-\Theta)+\frac{1}{4\pi}\frac{\gamma+\psi(1-\gamma)}{2-\gamma-\psi(1-\gamma)}\\ &\times\left[\frac{1-\psi}{2-\psi}\frac{8\gamma}{\gamma+\psi(1-\gamma)}\left(\frac{\Pi}{\Theta}\left(1-\frac{7}{4}\Theta\right)+\frac{1}{2}\sqrt{\Theta}\right)-(\Pi+2\sqrt{\Theta})\right]\frac{\Theta^{3/2}}{\Pi^2}\hat{J}^2+\frac{\psi}{2-\psi}\frac{1}{8\pi^2}\frac{\Theta^{5/2}}{\Pi^3}\hat{J}^4.\end{aligned}\tag{23}$$

The dimensionless eHKS equations depend only on temperature ratio, Θ, and pressure ratio, Π. Correspondingly, the dimensionless resistivities $\hat{r}_{\alpha\beta}$ will be independent of interface temperature T_l and saturation pressure $p_{\rm sat}(T_l)$, and depend only on the dimensionless fluxes $\hat{J},\hat{q}_v$. This simplified dependence of resistivities on system and process properties results from the vapor being modeled as an ideal gas.

D. Ytrehus-Cercignani interface model

For context and comparison we also consider a classical kinetic theory interface model that was originally developed by Ytrehus and Østmo [30] and subsequently refined by Cercignani [31]. In contrast to the eHKS model, the Y-C model accounts for the influence of Knudsen layers. However, the model was only developed for evaporation with zero heat flux

q_v in the vapor, and for a condensation coefficient of unity (hence the accommodation coefficient does not appear). With this, the Y-C model is both more refined, and more limited compared to the eHKS model.

Using the same dimensionless properties as above, the Y-C model can be written as a set of coupled nonlinear equations as follows.

The dimensionless vapor velocity is defined as

$$S_\infty = \frac{v_v}{\sqrt{2RT_v}} = \frac{1}{2\sqrt{\pi}}\frac{\sqrt{\Theta}}{\Pi}\hat{J}. \tag{24}$$

Temperature and pressure ratios are related to (24) through

$$\Theta = \left(\sqrt{\frac{\pi S_\infty^2}{64}} + 1 - \frac{\sqrt{\pi}S_\infty}{8}\right)^2, \quad \Pi = \frac{F + \sqrt{\Theta}G}{2\exp\left(-S_\infty^2\right)}, \tag{25}$$

with the abbreviations

$$F = -\sqrt{\pi}S_\infty(1 - \mathrm{erf}S_\infty) + \exp\left(-S_\infty^2\right), \tag{26}$$

$$G = \left(2S_\infty^2 + 1\right)(1 - \mathrm{erf}S_\infty) - \frac{2}{\sqrt{\pi}}S_\infty \exp\left(-S_\infty^2\right). \tag{27}$$

The relations (25) between mass flux and temperature and pressure ratios correspond to Eqs. (22) and (23) for vanishing heat flux, $\hat{q}_v = 0$.

III. DETERMINING RESISTIVITIES FROM MODELS

We proceed with the determination of resistivities from the eHKS and Y-C models, where we first consider the linear case, for which resistivities are constant, then nonlinear single-flux cases, then the general nonlinear case with both fluxes.

A. Linear resistivities

In the linear limit a first-order Taylor expansion of (22) and (23) with (14) in $\Delta\hat{p}$ and $\Delta\hat{T}$ and reordering into the form (16) yields the resistivities of the eHKS model in dependence of condensation and accommodation coefficients as [18,23,32]

$$\hat{r}_{\alpha\beta} = \begin{bmatrix} \frac{1}{\psi} - \frac{7}{16}\left(\frac{1-\frac{9}{7}(1-\gamma)(1-\psi)}{\gamma+\psi(1-\gamma)}\right) & \frac{1}{8}\left(\frac{2-\gamma-\psi(1-\gamma)}{\gamma+\psi(1-\gamma)}\right) \\ \frac{1}{8}\left(\frac{2-\gamma-\psi(1-\gamma)}{\gamma+\psi(1-\gamma)}\right) & \frac{1}{4}\left(\frac{2-\gamma-\psi(1-\gamma)}{\gamma+\psi(1-\gamma)}\right) \end{bmatrix}. \tag{28}$$

For the case of fully diffusive reflection, $\gamma = 1$, the resistivities reduce to

$$\hat{r}_{\alpha\beta} = \begin{bmatrix} \frac{1}{\psi} - \frac{7}{16} & 0.125 \\ 0.125 & 0.25 \end{bmatrix}. \tag{29}$$

These resistivity matrices are symmetric in agreement with the Onsager principle [35].

The Detailed derivation of the resistivities from the Boltzmann equation under the same assumptions yields slightly different values [11,12,42]:

$$\hat{r}^{\mathrm{KT}}_{\alpha\beta} = \begin{bmatrix} \frac{1}{\Psi} - 0.400\,44 & 0.126 \\ 0.126 & 0.2905 \end{bmatrix}, \tag{30}$$

in which Ψ is the condensation coefficient in this more refined model; it is often assumed that $\Psi = 1$ so that $\hat{r}^{\mathrm{KT}}_{11} \simeq 0.6$.

Since the Y-C model (24)–(27) is restricted to zero heat flux, $q_v = 0$, and $\Psi = 1$, one can only determine the resistivities $\hat{r}^{\text{Y-C}}_{11} = \hat{r}^{\mathrm{KT}}_{11} \simeq 0.6$ and $\hat{r}^{\text{Y-C}}_{21} = 0.125$; that is, the model is in agreement with the other kinetic theory results.

The difference between the eHKS model yielding (29) and the accurate kinetic theory models lies in the omission of Knudsen layers in the former. To offset the difference in $\hat{r}_{11}$ in the eHKS model (29) one can set its condensation coefficient to $\psi = 0.964$; this value was recently found also in [42]. While it is possible to adjust $\hat{r}_{11}$ to match the accurate model by selecting an appropriate interface coefficient, and the cross coefficients $\hat{r}_{12} = \hat{r}_{21}$ agree well without adjustment, it is not possible to adjust $\hat{r}_{22}$.

Nevertheless, the eHKS model describes the principal mass and heat-transfer behavior of the interface quite well; its explicit nonlinear relations provide a meaningful example to study nonlinearity in force-flux relations at the interface.

We emphasize that although the dimensionless kinetic theory resistivities $\hat{r}_{\alpha\beta}$ are constants, their dimensional counterparts $r_{\alpha\beta}$ in (10) depend strongly on temperature, both through the saturation pressure and directly. Therefore, we suggest evaluating the interface coefficients through dimensionless resistivities $\hat{r}_{\alpha\beta}$ to determine whether there is a nonlinear dependence on the fluxes beyond the effects of the temperature and saturation pressure.

B. Resistivities for single-flux cases ($\hat{q}_v = 0$ or $\hat{J} = 0$)

For nonlinear process conditions, the resistivities must be determined numerically based on the equations discussed above. This task is straightforward for single-flux cases, where either the mass flux $\hat{J}$ or the vapor heat flux $\hat{q}_v$ vanish. These settings are often used in MD simulations [15].

If the mass flux is nonzero, but the heat flux vanishes, Eq. (13) yields two resistivities as

$$\hat{r}_{11} = \frac{\hat{\mathcal{F}}_J(\Theta,\Pi)}{\hat{J}(\Theta,\Pi)}, \quad \hat{r}_{21} = \frac{\hat{\mathcal{F}}_q(\Theta,\Pi)}{\hat{J}(\Theta,\Pi)}, \tag{31}$$

where temperature and pressure ratios are related through the requirement of vanishing heat flux, $\hat{q}_v(\Theta,\Pi) = 0$, given by Eq. (23) with (22). Thus, one can prescribe a value of $\hat{J}$ (or Θ), determine the corresponding values of Θ (or $\hat{J}$) and Π from (22) and (23), and from these determine the forces $\hat{\mathcal{F}}_\alpha(\Theta,\Pi)$, and finally combine the results to find the resistivities as $\hat{r}_{11}(\hat{J}), \hat{r}_{21}(\hat{J})$. The resistivities for the Y-C model (24)–(27) are obtained in the same manner.

A corresponding strategy gives the resistivities $\hat{r}_{12}(\hat{q}_v), \hat{r}_{22}(\hat{q}_v)$ in the case of vanishing mass flux $\hat{J}$ from

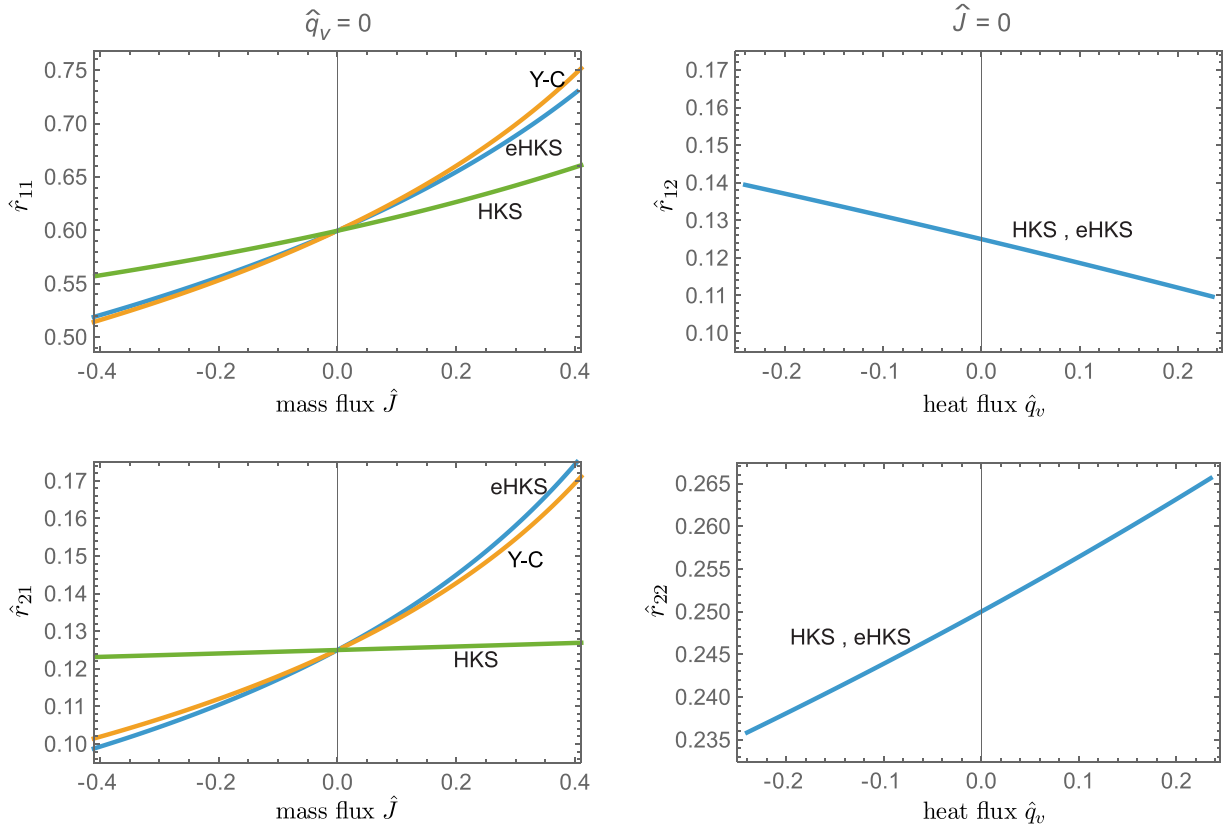

FIG. 3. Left: $\hat{r}_{11}$ and $\hat{r}_{21}$ as functions of mass flux $\hat{J}$ for pure mass transfer ($\hat{q}_v = 0$) for the eHKS (blue), Y-C (orange), and HKS (green) models. Right: $\hat{r}_{12}$ and $\hat{r}_{22}$ as functions of heat flux $\hat{q}_v$ for pure heat transfer ($\hat{J} = 0$) for the eHKS and HKS models. Condensation and accommodation coefficients are set to $\psi = 0.964$ and $\gamma = 1$ in order to match the Y-C model.

the equations

$$\hat{r}_{12} = \frac{\hat{\mathcal{F}}_J(\Theta, \Pi)}{\hat{q}_v(\Theta, \Pi)}, \quad \hat{r}_{22} = \frac{\hat{\mathcal{F}}_q(\Theta, \Pi)}{\hat{q}_v(\Theta, \Pi)}, \tag{32}$$

where Θ and Π are related by (22) with $\hat{J} = 0$.

As an example, Fig. 3 shows the eHKS resistivities for $\psi = 0.964$ and $\gamma = 1$, which are chosen to match the Y-C model in the linear limit. The two figures on the left indicate that the mass transfer resistivities $\hat{r}_{11}, \hat{r}_{21}$ are in very good agreement between eHKS and Y-C for the chosen range of mass fluxes, which is motivated by the MD simulations studied further below, while the original HKS model (17) deviates considerably. The figures on the right, for vanishing mass flux, show the identical heat-transfer resistivities $\hat{r}_{12}, \hat{r}_{22}$ for HKS and eHKS, which have no Y-C counterpart.

All resistivities are nonlinear functions of their respective fluxes.

Different choices of ψ and γ shift the four resistivities up or down, while largely preserving their nonlinear characteristics; some examples will be shown below in the comparison to MD results.

Notably, Onsager symmetry of the off-diagonal elements is observed only in the linear limit [35], since these resistivities are determined for different process conditions.

C. General nonlinear resistivities

1. Problem statement and setup

We proceed with the discussion of resistivities from eHKS for a wider range of process conditions with simultaneous mass and heat fluxes. Specifically, we aim to determine the dimensionless resistivities as a function of the fluxes, that is, $\hat{r}_{\alpha\beta}(\hat{J}, \hat{q}_v)$.

The resistivities are obtained from (13), which we write as

$$\hat{r}_{11}\hat{J}(\Theta, \Pi) + \hat{r}_{12}\hat{q}_v(\Theta, \Pi) - \hat{\mathcal{F}}_J(\Theta, \Pi) = 0, \tag{33}$$

$$\hat{r}_{21}\hat{J}(\Theta, \Pi) + \hat{r}_{22}\hat{q}_v(\Theta, \Pi) - \hat{\mathcal{F}}_q(\Theta, \Pi) = 0, \tag{34}$$

with the definitions of the forces given in (13). The eHKS fluxes as functions of Θ,Π are given in (22) and (23).

With two equations to determine four resistivities, Eqs. (33) and (34) do not have unique solutions as soon as both fluxes, $\hat{J}$ and $\hat{q}$, are different from zero. In these cases, there are infinitely many possible solutions for the nonlinear resistivities, which all obey (33) and (34) and include the nonambiguous single-flux results (31) and (32). Any of these solutions would properly relate the fluxes and the forces, hence there is no clear criterion of choice.

Below we present the determination of local (in $\hat{J}, \hat{q}_v$) resistivities from an optimization procedure that considers neighboring data points to find smooth solutions not too far from a global initial guess, which we chose as the equilibrium limit of the resistivities (28).

When the optimization is performed on Eqs. (33) and (34), each equation is treated independently; that is, (33) is used to determine $\hat{r}_{11}$,$\hat{r}_{12}$, and (34) is used to determine $\hat{r}_{21}, \hat{r}_{22}$. With that, Onsager symmetry cannot be expected, unless it is enforced.

Considering the arguments in Ref. [18] in favor of symmetry, we enforce symmetry by setting $\hat{r}_{21} = \hat{r}_{12}$ in (33) and (34). Elimination of $\hat{r}_{12}$ then leads to a relation between the diagonal resistivities, that we write as

$$E(\hat{r}_{11}, \hat{r}_{22}; \Theta, \Pi) = \frac{\hat{\mathcal{F}}_J(\Theta, \Pi) - \hat{r}_{11}\hat{J}(\Theta, \Pi)}{\hat{q}_v(\Theta, \Pi)} - \frac{\hat{\mathcal{F}}_q(\Theta, \Pi) - \hat{r}_{22}\hat{q}_v(\Theta, \Pi)}{\hat{J}(\Theta, \Pi)} = 0, \quad (35)$$

where E is the objective function for the optimization process. The equation $E = 0$ has infinitely many local solutions for $\hat{r}_{11}, \hat{r}_{22}$ that all guarantee symmetry. The corresponding off-diagonal resistivities are obtained from a solution as

$$\hat{r}_{12} = \hat{r}_{21} = \frac{\hat{\mathcal{F}}_J - \hat{r}_{11}\hat{J}}{\hat{q}_v} = \frac{\hat{\mathcal{F}}_q - \hat{r}_{22}\hat{q}_v}{\hat{J}}. \quad (36)$$

The optimization procedure is explained in the next section. We remark that with the inclusion of higher-order mass flux terms in the extended HKS fluxes (19) and (20), one might choose to include kinetic energy in the balance of energy (3), which changes the definition of the thermodynamic force $\hat{F}_J$. However, this change merely results in a different definition of the resistivity r_{11}, and is not considered here.

2. Optimization

The optimization considers a large array of data for fluxes and forces that is obtained from dimensionless temperature and pressure prescribed on a grid as

$$\Theta^i = 1 + \frac{i}{\alpha n}, \quad \Pi^j = 1 + \frac{j}{\alpha n} \qquad (i, j = -n, n), \quad (37)$$

with the corresponding forces and fluxes determined to create the array

$$\mathcal{D}_{n\times n} = \langle \Theta^i | \Pi^j | \mathcal{F}_J^{i,j} | \mathcal{F}_T^{i,j} | \hat{J}^{i,j} | \hat{q}_V^{i,j} \rangle_{\{i,j=-n,n\}}, \quad (38)$$

where $\mathcal{F}_J^{i,j} = \hat{\mathcal{F}}_J(\Theta^i, \Pi^j)$, etc.

The task at hand is determination of the local values of the resistivities either as

$$\hat{r}_{\alpha\beta}^{i,j} = \hat{r}_{\alpha\beta}(\Theta^i, \Pi^j), \quad (39)$$

or as the alternative, and preferred, form

$$\hat{r}_{\alpha\beta}^{i,j} = \hat{r}_{\alpha\beta}\big(\hat{J}^{i,j}, \hat{q}_v^{i,j}\big). \quad (40)$$

To cover a large range of conditions for fluxes and forces, we chose $n = 50$ and $\alpha = 3$. The equilibrium state, for which $i = j = 0$, is excluded, so that the data table contains $4n^2 = 10^4$ nonequilibrium data sets.

We employed an optimization algorithm from the open-source scipy package in python, which determines the resistivities $\hat{r}_{11}, \hat{r}_{22}$ as the local minimum of the multivariable objective function (35). The algorithm supports both unconstrained and constrained optimization, using algorithms such as Nelder-Mead, Broyden-Fletcher-Goldfarb-Shanno (BFGS), and Newton-CG for the former, and COBYLA, SLSQP, and trust-constr for the latter. The BFGS method, used in this problem, is a quasi-Newton optimizer that approximates Newton's method to iteratively minimize the objective function. It is efficient, well suited for medium-sized problems, and widely adopted for its good convergence properties. More detail is provided in the scipy Reference Guide [43]. The algorithm searches for solutions in the vicinity of an initial guess, for which we chose the near equilibrium resistivities (28). The off-diagonal resistivities are obtained from (36) after optimization.

The results found, while not unique, have properties that are either required or desirable: equilibrium limit and single-flux cases are properly obtained; the diagonal resistivities $\hat{r}_{11}$,$\hat{r}_{22}$ are positive, as is the determinant $\hat{r}_{11}\hat{r}_{22} - \hat{r}_{12}^2$, hence the matrix is positive definite in agreement with the second law of thermodynamics; the obtained resistivities are smooth functions of the fluxes $\hat{J}, \hat{q}_v$.

3. Results

With a distinct lack of accurate data from physical or MD experiments, comparison or fitting for the full range of fluxes is not possible. Hence, in this section we consider only cases with condensation coefficient $\psi = 0.964$ and accommodation coefficient $\gamma = 1$. All resistivities are determined through the optimization method described above.

As a first check of the optimization method, we consider the resistivities in the linear limit $\hat{J} \to 0, \hat{q}_v \to 0$, which the algorithm finds as

$$\hat{r}^{0,0}{}_{\alpha\beta} = \begin{bmatrix} 0.599\,998 & 0.124\,999 \\ 0.124\,999 & 0.250\,051 \end{bmatrix}. \quad (41)$$

These numbers are in excellent agreement with the analytical result (29); the maximum relative error is 0.02%.

Figure 4 shows a subset of the resistivities as functions of mass and heat fluxes, limited to dimensionless fluxes below $\sim|0.5|$ with clearly visible nonlinear behavior of all resistivities. The local mean-square error based on (33) and (34) lies below 10^{-13}; that is, these resistivities fully agree with the underlying eHKS relations.

We reiterate that this set of resistivities is just one possible solution, and is shown to emphasize that nonlinear behavior, which was already seen in the single-flux cases, is expected for liquid-vapor processes under strong nonequilibrium.

Alternative resistivities determined from (33) and (34) show similar characteristics (see [33] for a comparison to the results presented here).

D. Discussion

Physical experiments, such as those by Ward and coworkers [2,3,5,6] and Gatapova [13] are performed in the linear regime. However, as will be seen in the next section, conditions of considerable nonlinearity are easily encountered in MD simulations. The nonlinearity must be accounted for when evaluating the obtained data. Nonlinear resistivities provide an excellent means of data visualization for single-flux cases, where they are unique, but might be difficult to explore in the general two-flux case, due to the inherent nonuniqueness.

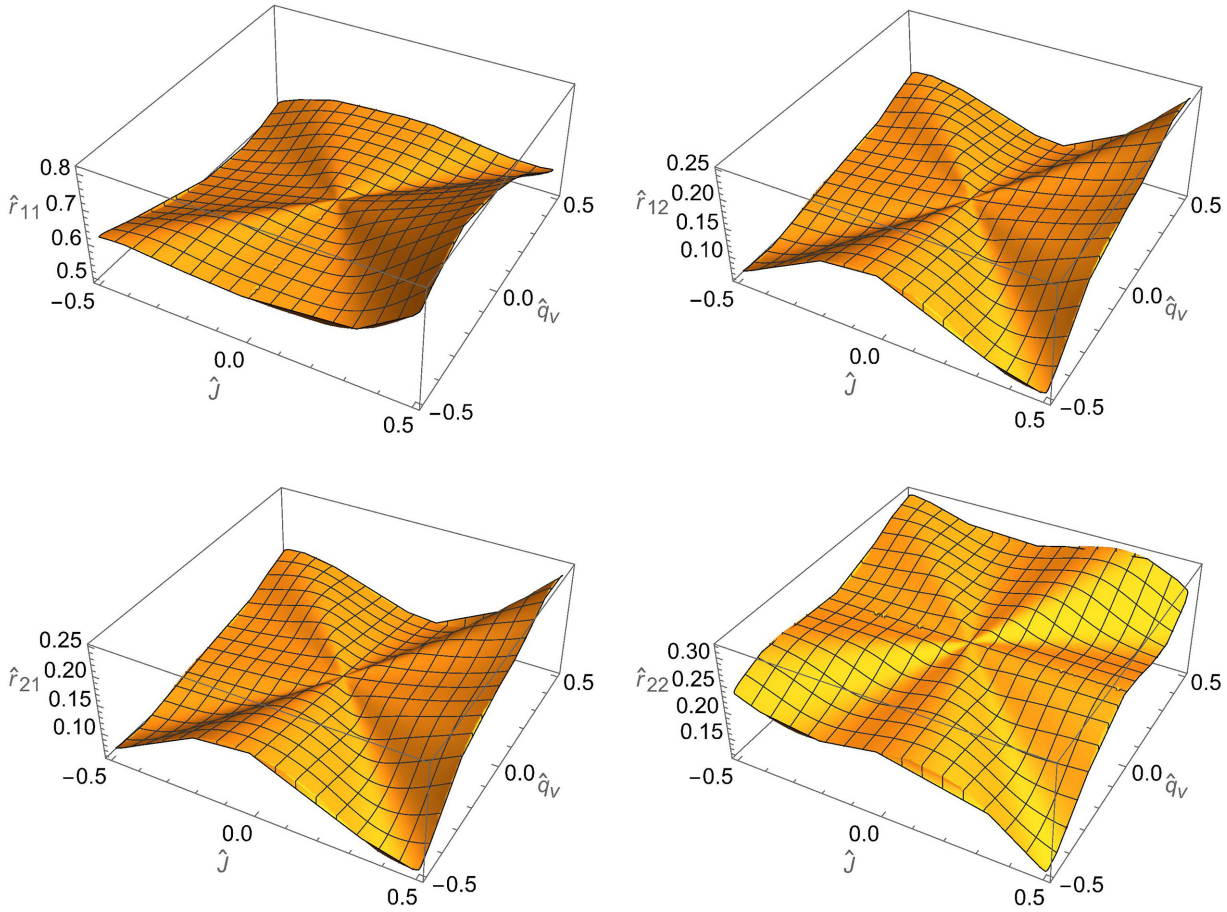

FIG. 4. Resistivities $\hat{r}_{\alpha\beta}$ for the eHKS model in dependence of mass and heat flux ($\psi = 0.964$, $\gamma = 1$).

IV. COMPARISON WITH MD DATA

A. Homes and Vrabec MD simulations

MD simulations provide a high-resolution alternative for studying interfaces with precise control over parameters such as evaporation flux and temperature gradients. These simulations require strong nonequilibrium conditions, with large evaporation fluxes and steep temperature gradients for heat transfer, to obtain data above the unavoidable stochastic noise [18,26]. As conditions approach equilibrium, noise effects increase, making it harder to extract meaningful transport properties. This trade-off complicates the determination of interface resistivities, as near-equilibrium simulations suffer from higher uncertainty due to the stochastic noise.

Recently, Homes and Vrabec performed a wide range of MD simulations for both single-flux cases and determined forces, fluxes, and resistivities from their data [15]. While in Ref. [15] the data is presented in figures, they provided their data tables for 44 evaporation and 36 heat-transfer scenarios, containing liquid and vapor temperatures T_l, T_v; pressure p and saturation pressure $p_{\mathrm{sat}}(T_l)$; mass flux J or heat flux q_v; and the dimensional resistivities $r_{\alpha\beta}$ obtained from their resolved process data. The original data is presented in dimensions suitable for simulations with the Lennard-Jones interaction potential, where certain microscopic parameters are set to unity (Lennard-Jones units).

In MD simulations the interface is resolved over an interval of several molecular diameters. The listed temperatures at the interface are obtained from extrapolation of the bulk temperatures to an assumed location of the sharp interface as explained in [15].

With the large gradients and fluxes applied in these simulations, this data is meaningful for the evaluation of nonlinear effects in evaporation, as well as showing the usefulness of studying the nondimensional forces, fluxes, and resistivities of Eqs. (10), (11), and (12).

Figure 5 presents Homes and Vrabec's original MD resistivities $r_{\alpha\beta}$ in Lennard-Jones units, with respect to the corresponding extrapolated liquid temperatures, measured relative to critical temperature T_{crit}. Note that this figure exhibits underlying stochastic noise, which is particularly evident for r_{11}. There is a strong dependence on temperature with a marked decrease in the values of all resistivities for larger temperatures.

In contrast, Fig. 6 presents the dimensionless resistivities $\hat{r}_{\alpha\beta}$ as introduced in Eq. (10), again with respect to the interface temperatures. Evidently, the multiplication with saturation pressure and powers of temperature required for nondimensionalization removes the exponential temperature

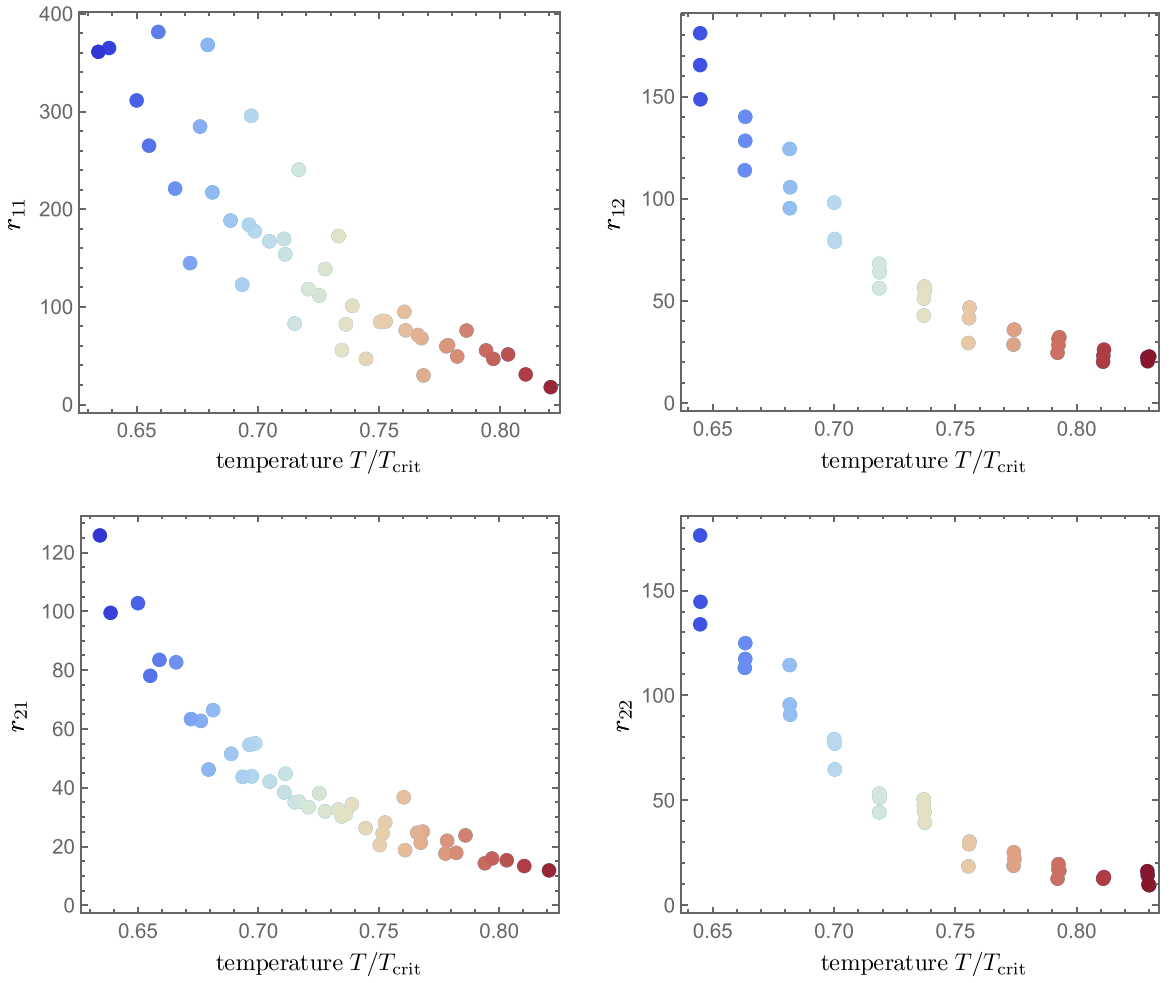

FIG. 5. Dimensional resistivities $r_{\alpha\beta}$ obtained from MD simulations as functions of liquid interface temperature [15].

behavior, which is thus seen to come from the saturation pressure. The dimensionless resistivities assume values of order unity or less in relatively compact intervals that are compatible with the kinetic theory results from the eHKS and Y-C models discussed above. The data is visibly affected by noise, which makes it impossible to identify well-defined values for the resistivities.

Onsager symmetry between $\hat{r}_{12}$ and $\hat{r}_{21}$ is not observed, which most likely is linked to the extrapolation of temperatures to the assumed location of the interface. As discussed in [38], the strong temperature gradients in simulations like this lead to a noticeable dependence of the values of resistivities on the interface location, where a shift of that location by a few atomic diameters can result in large variations of resulting resistivities (see Fig. 14 in [38]).

These two sets of figures consider resistivities as a function of temperature alone, as is usually assumed in LIT. With the gradients and fluxes large, and kinetic theory, e.g., the eHKS and Y-C models, suggesting nonlinear dependence on fluxes, we reconsider the dimensionless MD resistivities as functions of their respective fluxes in Fig. 7. The left subfigures show resistivities $\hat{r}_{11}$,$\hat{r}_{21}$ as functions of mass flux $\hat{J}$, while the right subfigures show resistivities $\hat{r}_{12}$,$\hat{r}_{22}$ as functions of heat flux $\hat{q}_v$. For all simulations mass flux is positive while heat flux is negative; that is, processes with stronger nonequilibrium are towards the right for evaporation, but towards the left for heat-transfer processes. In order to keep track of the associated liquid temperature the dots are color coded as in the previous figures.

Upon visual inspection, the resistivities appear more structured and follow a clearer pattern when plotted against their corresponding fluxes compared to the previous figures, where they were plotted against temperature.

For small values of mass flux, the resistivity $\hat{r}_{11}$ is strongly affected by noise and it is not possible to extract a meaningful value. However, at higher interface temperatures, the noise decreases. Both evaporation-related resistivities, $\hat{r}_{11}$ and $\hat{r}_{21}$, are slightly increasing with the mass flux, in principal agreement with what we have seen for the eHKS and Y-C models in Fig. 3.

For the heat-transfer-related resistivities, $\hat{r}_{12}$ and $\hat{r}_{22}$, higher interface temperatures are associated with lower heat-transfer rates and lower resistivities than at colder interfaces. As for the evaporation cases, noise is stronger for smaller (absolute) fluxes. One might be willing to observe a small negative slope for $\hat{r}_{12}$ similar to the eHKS curve in Fig. 3. For $\hat{r}_{22}$, temperature appears to play a more important role than for the other resistivities, with possibly positive slope for resistivities of similar temperature as in Fig. 3.

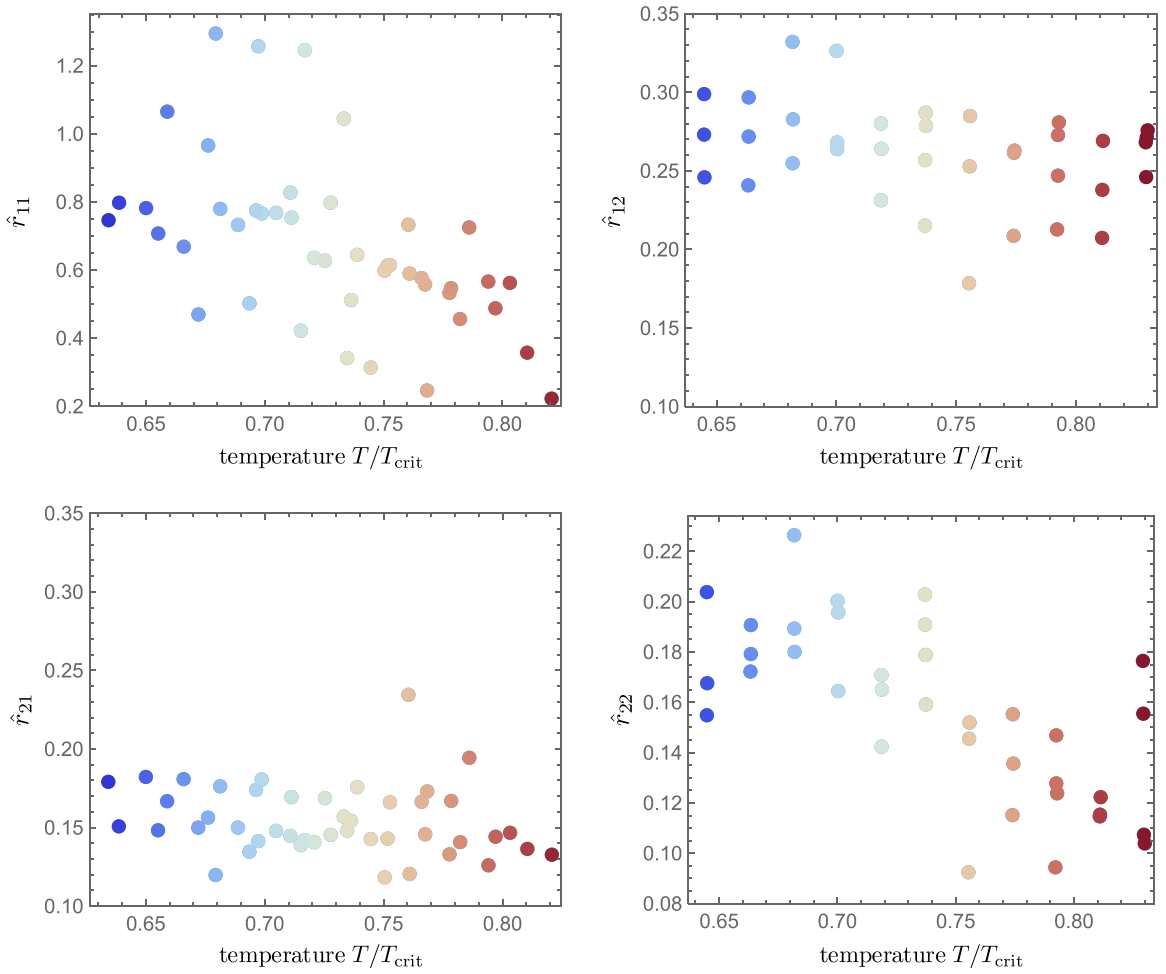

FIG. 6. Dimensionless resistivities $\hat{r}_{\alpha\beta}$ obtained from MD simulations of Ref. [15] as functions of liquid interface temperature.

B. Resistivities from eHKS and MD

The MD simulations cover temperatures up to $0.825T_{\mathrm{crit}}$. With the eHKS model valid for ideal gases, comparison is only meaningful for temperatures sufficiently below the critical temperature and thus we consider only data for temperatures below $0.76T_{\mathrm{crit}}$. Figure 8 compares the corresponding subset of resistivities obtained from MD with resistivities obtained from eHKS for several values of condensation and accommodation coefficients (green, purple, and orange curves), and the Y-C model (black).

As discussed earlier, the MD data does not obey Onsager symmetry, which, however, is inherent in the eHKS model. Accordingly, a proper fit of eHKS to MD is not possible, which implies that it is impossible to extract meaningful values for condensation and accommodation coefficients. Instead we used a few sets of parameters to visually indicate the principal agreement between MD and kinetic theory results.

The green curves rely on $\psi = 0.964, \gamma = 1$ to match the Y-C model (shown in black for $\hat{r}_{11}$,$\hat{r}_{21}$), which both show reasonable agreement for the evaporation case, in particular for lower temperatures. The orange curves, for $\psi = 0.6, \gamma = 0.1$, provide a good fit for the heat-transfer off-diagonal resistivity $\hat{r}_{12}$ while strongly overestimating the other resistivities. Similarly, the red curves, for $\psi = 1.2, \gamma = 0.4$, show a reasonable fit for $\hat{r}_{22}$ while underestimating the other resistivities. Moreover, the purple curves, for $\psi = 0.8, \gamma = 0.4$, are an attempt at having a somewhat balanced mismatch for all resistivities.

The eHKS model describes the mass flux dependence of $\hat{r}_{11}$ and $\hat{r}_{21}$ observed in MD reasonably well. Correspondingly, the (relatively weak)slopes for the heat-transfer resistivities $\hat{r}_{12}$ and $\hat{r}_{22}$ appear to match those observed in MD. However, the MD data for $\hat{r}_{22}$ are smaller than for all kinetic theory models, while those for $\hat{r}_{12}$ are comparatively large. It is likely that these deviations of resistivities are related to the positioning of the sharp interface in the temperature extrapolation that is necessary to extract resistivities from the MD data with resolved interface.

V. CONCLUSIONS

In this contribution, we explored nonlinearities in nonequilibrium mass and heat transfer across liquid-vapor interfaces by means of irreversible thermodynamics and the kinetic theory of gases.

Microscopically, in these processes imposed mass and heat fluxes induce temperature jumps across the interface as well as deviations from saturation pressure. Thermodynamic and

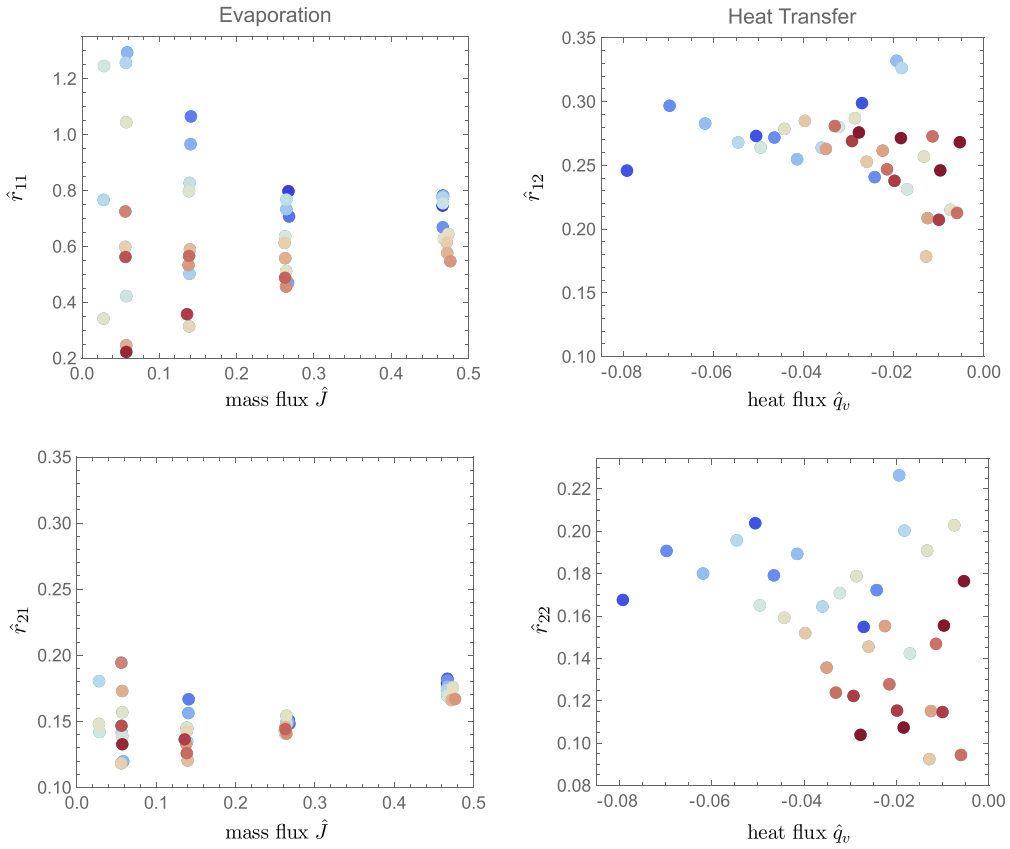

FIG. 7. Dimensionless resistivities $\hat{r}_{\alpha\beta}$ obtained from MD simulations of Ref. [15] as functions of mass or heat flux; color indicates interface temperatures.

kinetic theory models link fluxes and jumps, and the goal is to better understand these linkages, which in thermodynamics are described through interfacial resistivities, and in kinetic theory through condensation and accommodation coefficients, which then appear in macroscopic relations such as the HKS model.

Condensation and accommodation coefficients describe microscopic processes, and cannot be measured directly, but, just as resistivities, must be inferred from macroscopic observation, either in physical experiments, or microscopic simulations, e.g., MD. This requires a deep understanding of the processes, as well as of the models that are used for fitting.

Typically, resistivities are considered to depend only on interface temperature, independent of fluxes. However, thermodynamic arguments [18] and kinetic theory models lead to nonlinear models for evaporation and heat transfer under strong nonequilibrium conditions. Physical experiments typically are performed close to equilibrium, and nonlinear effects are not expected. Molecular Dynamics simulations are most reliable under strong nonequilibrium, where stochastic noise is relatively small, while close-to-equilibrium simulations are heavily affected by noise.

We have derived and presented the eHKS model as the nonlinear extension of the classical HKS equation for mass flux and the accompanying relation for vapor heat flux, which is too often ignored when discussing interface behavior. As a kinetic theory model, the eHKS model is explicit in condensation and accommodation coefficients. For processes with zero heat flux, and with properly adjusted coefficients, the eHKS model agrees well with the Ytrehus-Cercignani model for evaporation, which, however has no counterpart for heat-transfer processes.

For the example of eHKS, we have shown that extraction of flux-dependent resistivities from nonlinear models (or, in principle, experiments)yields meaningful unique results for single-flux cases, where either mass or heat flux vanish. However, for general cases with mass *and* heat flux it is not possible to find unique resistivities. Nevertheless, continuous functions for resistivities can be obtained from optimization of eHKS data (or, possibly, large sets of detailed measurements), that, however, are not unique, and thus might have practical value, but do not offer insight into the underlying physics.

For clear discussion and proper comparison of models from thermodynamics or kinetic theory, as well as experimental data, it is highly useful to nondimensionalize mass and heat fluxes, thermodynamic forces, and resistivities, where the proper nondimensionalization is guided by kinetic theory models. As long as the vapor is an ideal gas, this yields relations that are independent of the interface temperature, which allows one to directly compare data obtained under different interface temperatures and other process conditions.

In particular, nondimensionalization showed its value in the evaluation of MD resistivity data, where dimensionless resistivities are found in relatively narrow intervals in reasonably good agreement with values obtained from eHKS. Reordering and plotting relative to (dimensionless) fluxes

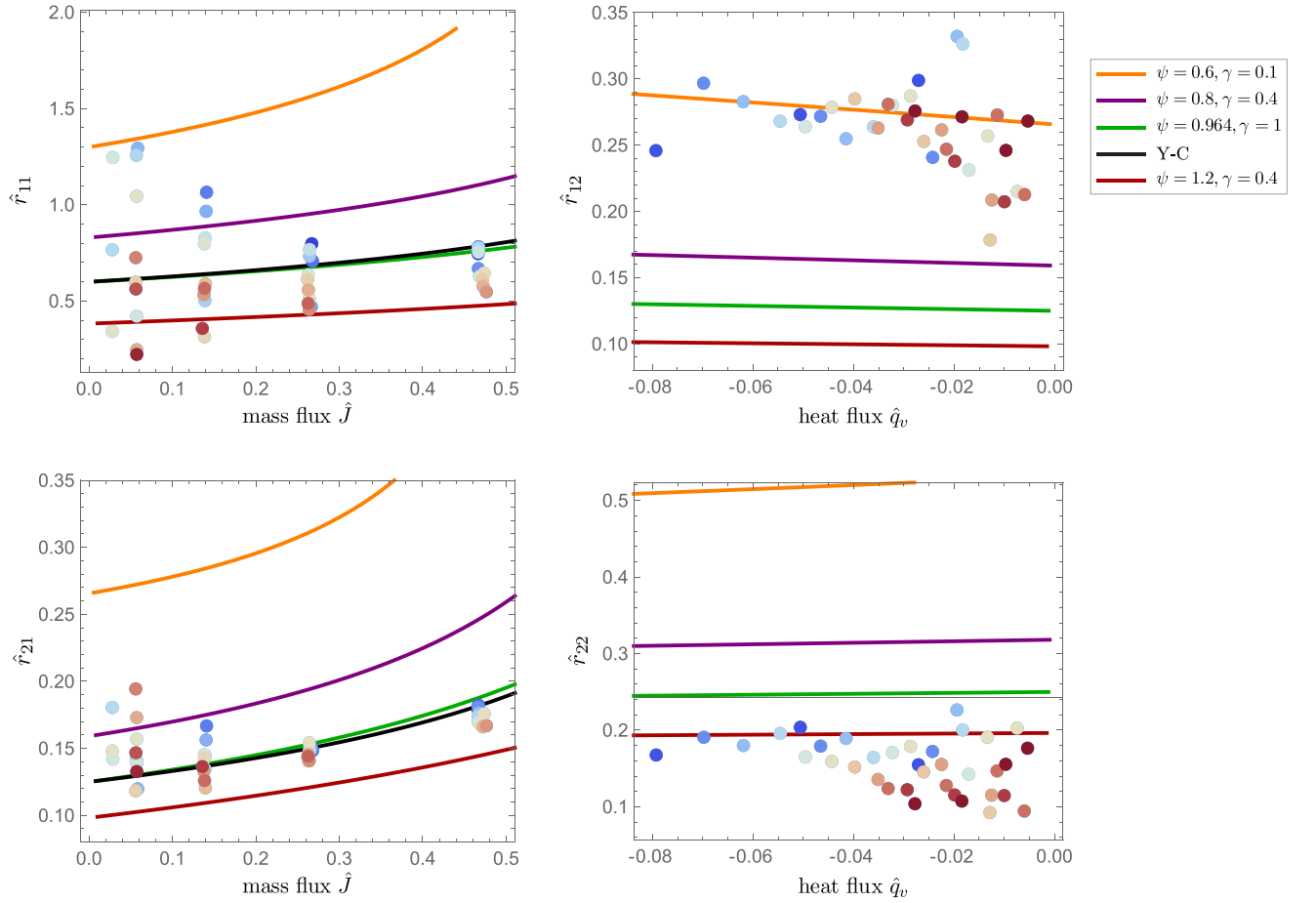

FIG. 8. Resistivity comparison: the points represent selected data from MD simulations colored based on their interface temperature [15], the Y-C model is shown in black, and the eHKS model with different coefficients in green, purple, and orange.

shows clear nonlinear behavior of MD resistivities, albeit with considerable noise. We argued that MD resistivities are affected by extrapolation of bulk temperatures to the assumed location of the interface, where small shifts in that location lead to marked changes of resistivities. This behavior is due to the strong deviation from equilibrium, which implies strong temperature gradients—another nonlinear effect. This likely explains the apparent violation of Onsager symmetry, as well as unresolvable discrepancies to eHKS for all choices of the microscopic coefficients. We conclude that nonlinearity must be carefully considered in the evaluation of MD simulations.

Future work in this realm should consider improvement of the eHKS model to account for Knudsen layer effects, reconsideration of MD data to adjust assumed interface location and reevaluation of resistivities, development of insightful alternatives to resistivities to study and visualize nonlinear effects at interfaces, and inclusion of real gas effects that influence interfacial behavior closer to the critical point.

ACKNOWLEDGMENTS

We thank Simon Homes and Jadran Vrabec for providing their detailed Molecular Dynamics data from Ref. [15], and James McDonald for asking important and helpful questions. The authors gratefully acknowledges support from the Natural Sciences and Engineering Research Council of Canada (NSERC) through Discovery Grant No. RGPIN-2022-03188.

DATA AVAILABILITY

The data that support the findings of this article are not publicly available upon publication because it is not technically feasible and/or the cost of preparing, depositing, and hosting the data would be prohibitive within the terms of this research project. The data are available from the authors upon reasonable request.

APPENDIX A: SIMPLIFICATION OF THE MASS TRANSFER FORCE

In this Appendix, we briefly show the simplification of the thermodynamic force for mass flux when the vapor is an ideal gas and the liquid is incompressible. The thermodynamic force for mass flux (8) reads

$$\mathcal{F}_J = \frac{g_l}{T_l} - \frac{g_v}{T_v} + h_v\left(\frac{1}{T_v} - \frac{1}{T_l}\right). \tag{A1}$$

The Gibbs free energy of the liquid $g_l = g_l(T_l, p)$ can be rewritten as $g_l(T_l, p_{\text{sat}}(T_l) + \Delta p)$, where pressure deviation for the liquid phase is defined as $\Delta p = p - p_{\text{sat}}(T_l)$. Taylor

expansion yields

$$g_l(T_l, p_{\rm sat}(T_l) + \Delta p) = g_l(T_l, p_{\rm sat}(T_l)) + \left(\frac{\partial g_l}{\partial p}\right)_{T_l, p_{\rm sat}(T_l)} \Delta p + \left(\frac{\partial^2 g_l}{\partial p^2}\right)_{T_l, p_{\rm sat}(T_l)} \Delta p^2 + \cdots . \quad \text{(A2)}$$

From the Gibbs equation follows the thermodynamic property relation [1],

$$\left(\frac{\partial g_l}{\partial p}\right)_{T_l, p_{\rm sat}(T_l)} = \mathsf{v}_l(T_l, p_{\rm sat}(T_l)) = \mathsf{v}_l^{\rm sat}(T_l), \quad \text{(A3)}$$

where v_l is the specific volume of the liquid phase, which for an incompressible liquid is independent of pressure; thus higher expansion terms in (A2) vanish, so that

$$g_l(T_l, p) = g_v^{\rm sat}(T_l) + RT_l \frac{\mathsf{v}_l^{\rm sat}(T_l)}{\mathsf{v}_v^{\rm sat}(T_l)} \frac{\Delta p}{p_{\rm sat}(T_l)}, \quad \text{(A4)}$$

where we have used the equilibrium condition $g_v^{\rm sat}(T_l) = g_l^{\rm sat}(T_l)$, and the ideal gas law for the saturation state as $p_{\rm sat}(T_l)\mathsf{v}_v^{\rm sat}(T_l) = RT_l$; where R is the gas constant. Inserting (A4) into (A1), together with $g = h - Ts$ yields

$$\mathcal{F}_J = \frac{h_v^{\rm sat}(T_l) - h_v(T_v)}{T_l} + s_v(T_v, p_v) - s_v^{\rm sat}(T_l) + R\frac{\mathsf{v}_l^{\rm sat}(T_l)}{\mathsf{v}_v^{\rm sat}(T_l)} \frac{\Delta p}{p_{\rm sat}(T_l)}. \quad \text{(A5)}$$

For a monatomic gas the enthalpy depends only on temperature,

$$h_v^{\rm sat}(T_l) - h_v(T_v) = \tfrac{5}{2}R(T_l - T_v), \quad \text{(A6)}$$

and entropy is given by

$$s_v(T_v, p_v) - s_v^{\rm sat}(T_l) = R\left[\frac{5}{2}\ln\frac{T_v}{T_l} - \ln\frac{p}{p_{\rm sat}(T_l)}\right]. \quad \text{(A7)}$$

With this we find the compact form

$$\mathcal{F}_J = R\left[\frac{5}{2}\left(1 - \frac{T_v}{T_l} + \ln\frac{T_v}{T_l}\right) - \ln\frac{p_v}{p_{\rm sat}(T_l)}\right]; \quad \text{(A8)}$$

the dimensionless force in (13) is $\hat{\mathcal{F}}_J = \mathcal{F}_J/R$.

APPENDIX B: eHKS KINETIC THEORY MODEL

The derivation of the original HKS model (17), (18) is discussed in Ref. [23], based on Maxwell's classical interface model [19] with a velocity-based condensation coefficient [25]. We extend that derivation by considering higher-order terms in mass flux in the distribution function, which were ignored in [23]. The distribution function is obtained from Chapman-Enskog (CE) expansion but ignoring viscous stresses.

Typically, the CE distribution is written in terms of the peculiar velocity $C_i = c_i - v_i$ of gas particles [19], where c_i is the particle velocity in the laboratory frame and v_i is the flow velocity of the gas. For the evaluation of interfacial transport, it is convenient to consider the distribution function in terms of the velocity c_i in a frame where the interface is at rest, which includes an expansion of the local Maxwellian into the rest frame of the interface [23].

Following [23], but expanding the Maxwellian to higher order, the appropriate approximation for the distribution function for one-dimensional transport in direction x is obtained as

$$f_{\rm CE} = f_M(p, T, c)\left\{1 + \frac{c_x J}{p} + \frac{1}{2}\frac{J^2}{p^2}\left(c_x^2 - RT\right) + \frac{1}{6}\frac{J^3}{p^3}c_x\left(c_x^2 - 3RT\right) + \frac{2}{5}\frac{qc_x}{pRT^2}\left(\frac{c^2}{2} - \frac{5}{2}RT\right)\right\}, \quad \text{(B1)}$$

where c_i is the particle velocity in the rest frame of the interface, T is local temperature, and

$$f_M(p, T, c) = \frac{p}{mRT}\frac{1}{(2\pi RT)^{3/2}}\exp\left[-\frac{c^2}{2RT}\right] \quad \text{(B2)}$$

is the Maxwellian distribution function in that frame; m denotes particle mass.

Notably, the distribution function (B1) reproduces the proper moments for the conservation laws of mass, momentum, and energy including all nonlinear contributions in flow velocity v. Specifically, mass density, momentum density (= mass flux), and total energy density (internal + kinetic) are obtained as

$$\rho = \frac{p}{RT} = m\int f_{\rm CE} d\mathbf{c}, \quad \text{(B3)}$$

$$\rho v = J = m\int c_x f_{\rm CE} d\mathbf{c}, \quad \text{(B4)}$$

$$\rho\left(\frac{3}{2}RT + \frac{v^2}{2}\right) = \frac{3}{2}p + \frac{1}{2}\frac{RT}{p}J^2 = m\int \frac{1}{2}c^2 f_{\rm CE} d\mathbf{c}. \quad \text{(B5)}$$

Moreover, momentum and energy flux are obtained with all velocity contributions as

$$p + \rho v^2 = p + \frac{RT}{p}J^2 = m\int c_x^2 f_{\rm CE} d\mathbf{c}, \quad \text{(B6)}$$

$$Q = \rho\left(\frac{5}{2}RT + \frac{v^2}{2}\right)v + q = \left(\frac{5}{2}RT + \frac{1}{2}\frac{RT}{p^2}J^2\right)J + q = m\int \frac{1}{2}c^2 c_x f_{\rm CE} d\mathbf{c}. \quad \text{(B7)}$$

The phase density (B1) was used to determine the expressions for mass and heat flux (19) and (20) following the procedure outlined and used in Ref. [23], with computations performed by the analytical mathematical software *Mathematica*. A helpful relation used along the way was

$$q + \frac{1}{2}\frac{RT}{p^2}J^3 = m\int\left(\frac{1}{2}c^2 c_x - \frac{5}{2}RT\right)c_x f_{\rm CE} d\mathbf{c}. \quad \text{(B8)}$$

This approach to determine the interface conditions for condensing and evaporating interfaces simplifies the actual physical conditions by neglecting Knudsen layers at the interface [31]. Although this introduces a minor error in the analysis, the results remain valid, useful, and reliable.

[1] H. Struchtrup, *Thermodynamics and Energy Conversion*, 2nd ed. (Springer, New York, 2024).

[2] G. Fang and C. A. Ward, Temperature measured close to the interface of an evaporating liquid, Phys. Rev. E **59**, 417 (1999).

[3] C. A. Ward and D. Stanga, Interfacial conditions during evaporation or condensation of water, Phys. Rev. E **64**, 051509 (2001).

[4] V. K. Badam, V. Kumar, F. Durst, and K. Danov, Experimental and theoretical investigations on interfacial temperature jumps during evaporation, Exp. Therm. Fluid Sci. **32**, 276 (2007).

[5] M. Kazemi and C. A. Ward, Assessment of the statistical rate theory expression for evaporation mass flux, Int. J. Heat Mass Transfer **179**, 121709 (2021).

[6] A. Persad and C. A. Ward, Expressions for the evaporation and condensation coefficients in the Hertz-Knudsen relation, Chem. Rev. **116**, 7727 (2016).

[7] P. Jafari, A. Amritkar, and H. Ghasemi, Temperature discontinuity at an evaporating water interface, J. Phys. Chem. C **124**, 1554 (2020).

[8] H. Hertz, Über die Verdunstung der Flüssigkeiten, insbesondere des Quecksilbers, im luftleeren Raume, Ann. Phys. (NY) **253**, 177 (1882).

[9] M. Knudsen, Die maximale Verdampfungsgeschwindigkeit des Quecksilbers, Ann. Phys. (NY) **352**, 697 (1915).

[10] R. W. Schrage, *A Theoretical Study of Interphase Mass Transfer* (Columbia University Press, New York, 1953).

[11] Y. Pao, Application of kinetic theory to the problem of evaporation and condensation, Phys. Fluids **14**, 306 (1971).

[12] J. Cipolla, Jr., H. Lang, and S. Loyalka, Kinetic theory of condensation and evaporation. II, J. Chem. Phys. **61**, 69 (1974).

[13] E. Y. Gatapova, Evaporation into half-space: Experiments with water at the molecular mean free path scale, Phys. Fluids **36**, 091707 (2024).

[14] M. Rauter, A. Aasen, S. Kjelstrup, and Ø. Wilhelmsen, A comparative study of experiments and theories on steady-state evaporation of water, Chem. Thermodyn. Therm. Anal. **8**, 100091 (2022).

[15] S. Homes and J. Vrabec, Resistivities across the vapor–liquid interface of a simple fluid: An assessment of methods, Phys. Fluids **36**, 022122 (2024).

[16] S. Homes, M. Heinen, J. Vrabec, and J. Fischer, Evaporation driven by conductive heat transport, Mol. Phys. **119**, e1836410 (2021).

[17] S. Kjelstrup and D. Bedeaux, *Non-equilibrium Thermodynamics of Heterogeneous Systems* (World Scientific, Singapore, 2008).

[18] H. Struchtrup and H. C. Öttinger, Nonequilibrium liquid-vapor interfaces: Linear and nonlinear descriptions, Phys. Rev. E **108**, 064801 (2023).

[19] H. Struchtrup, *Macroscopic Transport Equations for Rarefied Gas Flows* (Springer, New York, 2005).

[20] H. Struchtrup and A. Frezzotti, Twenty-six moment equations for the Enskog–Vlasov equation, J. Fluid Mech. **940**, A40 (2022).

[21] Y. Sone and Y. Onishi, Kinetic theory of evaporation and condensation hydrodynamic equation and slip boundary condition, J. Phys. Soc. Jpn. **44**, 1981 (1978).

[22] Y. Sone, *Kinetic Theory and Fluid Dynamics* (Springer, New York, 2002).

[23] J. Caputa and H. Struchtrup, Interface model for non-equilibrium evaporation, Phys. A (Amsterdam, Neth.) **390**, 31 (2011).

[24] K. Yasuoka, M. Matsumoto, and Y. Kataoka, Evaporation and condensation at a liquid surface. I. Argon, J. Chem. Phys. **101**, 7904 (1994).

[25] T. Tsuruta, H. Tanaka, and T. Masuoka, Condensation/evaporation coefficient and velocity distributions at liquid-vapor interface, Int. J. Heat Mass Transfer **42**, 4107 (1999).

[26] R. Meland, A. Frezzotti, T. Ytrehus, and B. Hafskjold, Nonequilibrium molecular-dynamics simulation of net evaporation and net condensation, and evaluation of the gas-kinetic boundary condition at the interphase, Phys. Fluids **16**, 223 (2004).

[27] T. Ishiyama, T. Yano, and S. Fujikawa, Molecular dynamics study of kinetic boundary condition at an interface between argon vapor and its condensed phase, Phys. Fluids **16**, 2899 (2004).

[28] T. Ishiyama, T. Yano, and S. Fujikawa, Kinetic boundary condition at a vapor-liquid interface, Phys. Rev. Lett. **95**, 084504 (2005).

[29] H. Struchtrup, *A Thermodynamic Introduction to Transport Phenomena* (Springer, New York, 2024).

[30] T. Ytrehus and S. Østmo, Kinetic theory approach to interphase processes, Int. J. Multiphase Flow **22**, 133 (1996).

[31] C. Cercignani, Strong evaporation of a polyatomic gas, in *12th International Symposium on Rarefied Gas Dynamics, Technical Papers, Part 1* (American Institute of Aeronautics and Astronautics, New York, 1981), pp. 305–320.

[32] M. Bond and H. Struchtrup, Mean evaporation and condensation coefficients based on energy dependent condensation probability, Phys. Rev. E **70**, 061605 (2004).

[33] P. F. Oskouei, Nonlinear heat and mass transfer resistivities for liquid-vapor interfaces, Master's thesis, University of Victoria, Victoria, BC, Canada, 2025.

[34] S. R. De Groot and P. Mazur, *Non-equilibrium Thermodynamics* (Dover, New York, 1984).

[35] F. Sharipov, Onsager-casimir reciprocity relations for open gaseous systems at arbitrary rarefraction: II. Application of the theory for single gas, Physica A (Amsterdam, Neth.) **203**, 457 (1994).

[36] V. Roldughin and V. Zhdanov, Non-equilibrium thermodynamics and kinetic theory of gas mixtures in the presence of interfaces, Adv. Colloid Interface Sci. **98**, 121 (2002).

[37] H. C. Öttinger, *Beyond Equilibrium Thermodynamics* (Wiley, New York, 2005).

[38] H. Struchtrup, H. Jahandideh, A. Couteau, and A. Frezzotti, Heat transfer and evaporation processes from the Enskog-Vlasov equation and its moment equations, Int. J. Heat Mass Transfer **223**, 125238 (2024).

[39] H. Homes, A. Frezzotti, I. Nitzke, H. Struchtrup, and J. Vrabec, Heat and mass transfer across the vapor-liquid interface: A comparison of molecular dynamics and the Enskog-Vlasov

Kinetic model, Int. J. Heat Mass Transfer **242**, 126828 (2025).

[40] S. Fujikawa, T. Yano, and M. Watanabe, *Vapor-Liquid Interfaces, Bubbles and Droplets* (Springer, New York, 2011).

[41] T. Ytrehus, Molecular-flow effects in evaporation and condensation at interfaces, Multiphase Sci. Technol. **9**, 205 (1997).

[42] E. S. Benilov, Surprisingly high probability of evaporation for a molecule passing through the Knudsen layer, Phys. Rev. E **111**, 044116 (2025).

[43] P. Virtanen, R. Gommers, T. Oliphant, M. Haberland, T. Reddy, D. Cournapeau, E. Burovski, P. Peterson, W. Weckesser, J. Bright *et al.*, Scipy 1.0: fundamental algorithms for scientific computing in python, Nat. Methods **17**, 261 (2020).